This is a post-peer-review, pre-copyedit version of an article published in Wear. J.M. Shockley, E.F. Rauch, R.R. Chromik, S. Descartes, "TEM microanalysis of interfacial structures after dry sliding of cold sprayed Al-Al2O3," Wear 376, 1411-17 (2017) at DOI: 10.1016/j.wear.2016.12.052

TEM microanalysis of interfacial structures after dry sliding of cold sprayed Al-Al2O3

J. Michael Shockley[1,2], E.F. Rauch[3], R.R. Chromik[1], S. Descartes[2]

[1]Department of Mining and Materials Engineering, McGill University, Montreal, QC Canada
[2]LaMCoS, UMR 5259, CNRS, INSA-Lyon, 69621 Villeurbanne, France
[3]SIMaP, UMR 5266, CNRS, Grenoble INP, 38402 Saint Martin d'Hères, France

Abstract

Particle-reinforced aluminum matrix composites (Al-MMCs) generally exhibit lower wear rates and more stable friction than their un-reinforced matrix materials. Cold spray is a popular consolidation route for Al-Al2O3, allowing for its application as a coating for corrosion and tribological protection. Previous work by the authors has found that 22 wt.% of angular Al2O3 particles (sample ANG22) leads to significantly decrease third body source flow and recirculation third body flow leading to decrease drastically wear flow and thus lower wear rates. The greater friction stability in the case of ANG22 during dry sliding against sapphire compared to unreinforced pure Al cold sprayed coatings (sample CS0) [2,3] is attributed to a specific thin third body to be characterized. Thus the goal of the present work is to study the near-surface third body material for CS0 and ANG22 in terms of microstructure and chemistry, studied through transmission electron microscopy (TEM) methods, related to its hardness.

This is a post-peer-review, pre-copyedit version of an article published in Wear. J.M. Shockley, E.F. Rauch, R.R. Chromik, S. Descartes, "TEM microanalysis of interfacial structures after dry sliding of cold sprayed Al-Al2O3," Wear 376, 1411-17 (2017) at DOI: 10.1016/j.wear.2016.12.052

1 Introduction

The cold spray process is one among many deposition processes for coatings made of pure aluminum, which are valued for their corrosion resistance in aerospace and other industrial sectors [1]. Cold spray is particularly advantageous in that it induces minimal heating of the substrate material during deposition, and also readily allows for deposition of multi-phase coatings by admixing feedstock powders [2, 3]. Thus aluminum matrix composite (Al-MMC) coatings, which incorporate hard phases such as Al2O3 or SiC, may be cold sprayed onto a wide variety of substrate materials. Cold sprayed Al-MMC coatings have been shown to maintain aluminum's corrosion resistance while substantially lowering wear rates [3], the latter being the role of hard particles in Al-MMCs [4, 5, 6, 7].

When subject to sliding wear in the mild wear regime, hard particle reinforced Al-MMCs often exhibit lower wear rates compared to their un-reinforced matrix materials [8]. The mechanisms by which this occurs is generally attributed to the formation of a third body layer, sometimes referred to as a mechanically mixed layer, which is hardened surface material which may contain plastically deformed aluminum, components of the counterface material, fragmented reinforcement particles, oxidized aluminum matrix material, and/or components of any lubricant present [8, 6, 4]. In cold sprayed Al- 22 wt.% Al2O3 subject to dry sliding, the third body layer has been shown to form in layers 2-5 μm thick, with distinct boundaries between the third body layer and the surrounding first body material [9, 10, 11]. In comparison, sliding on unreinforced cold sprayed pure aluminum results in plastic deformation extending deeper into the wear track, and adhesive wear occurs. The underlying mechanisms behind this contrasting behavior remain somewhat poorly understood, and unanswered questions on the microstructure evolution of third body layers remain [10].

In the present study, transmission electron microscopy (TEM) was conducted on third body layers after dry sliding on cold sprayed commercially pure Al and Al- 22 wt.% Al_2O_3 subjected to dry sliding wear against sapphire. Automated crystal orientation mapping (ACOM) in the TEM provided high resolution phase identification and grain size quantification. This microstructural analysis revealed differing sliding-induced material transformation processes in the Al vs. the Al-Al2O3 third bodies.

2 Experimental

Two batches of feedstock powder were prepared, one consisting entirely of commercially available spherical Al powder (Valimet H-15, d50= 22.57 μm), while the other was an admixture of the latter with Al2O3 powder with angular morphology (Plasmatec, d50= 25.5 μm) at a concentration of 50 wt.% (see Figure 1). Coatings were deposited onto aluminum alloy AA6061 substrates using a Plasma Giken PCS-800 cold spray system, achieving a thickness of 4-5 mm. A nitrogen carrier gas was used at a 400°C chamber temperature and 3 MPa chamber pressure. Additional details of the cold spray process can be found in a previous publication by the authors [11].

This is a post-peer-review, pre-copyedit version of an article published in Wear. J.M. Shockley, E.F. Rauch, R.R. Chromik, S. Descartes, "TEM microanalysis of interfacial structures after dry sliding of cold sprayed Al-Al2O3," Wear 376, 1411-17 (2017) at DOI: 10.1016/j.wear.2016.12.052

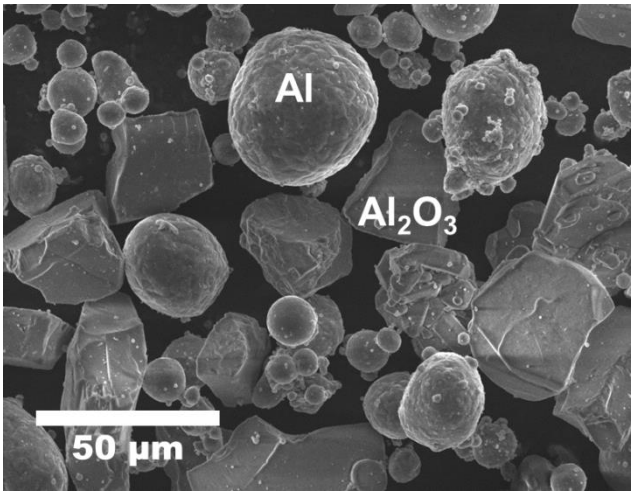

Figure 1: Admixed feedstock powder showing spherical Al and angular Al2O3 particles

Microstructures of the cold sprayed coatings were revealed using metallographic polishing and revealed that the coatings were of high density, with a porosity of less than 2% (see Figure 2). The Vickers microhardness of the pure aluminum coating ("CS0") was 53.4 HV_{200} ± 1.7. The Al-Al2O3 coating ("ANG22") was found to contain 22 wt.% Al2O3, as measured by image analysis of backscattered electron (BSE) scanning electron microscopy (SEM) images and had a microhardness of 78.9 HV_{200} ± 4.7.

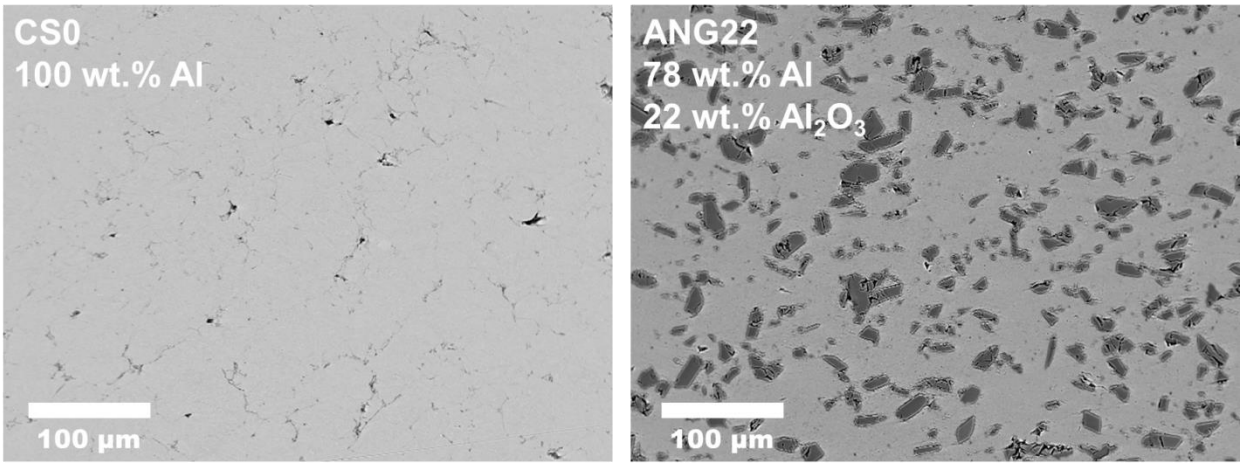

Figure 2: Initial unworn microstructures of the pure aluminum and Al-Al2O3 composite coatings

Dry sliding wear tests on the prepared coatings were performed in dry air (below 1% relative humidity) at room temperature (21-24° C). All tests were conducted with a sliding speed of 3 mm/s, a track length of 10 mm, and normal load of 1 N. Friction forces were measured at a sampling rate of 800 Hz using a piezoelectric sensor mounted underneath the sample stage. Monocrystalline a-Al_2O_3(sapphire) spheres of 6.35 mm diameter were used as the counterface material. The samples in this study were subject to thorough dry sliding wear testing and analysis in a previous study [11] and for the sake of this study were subject to one sliding wear test to 500

This is a post-peer-review, pre-copyedit version of an article published in Wear. J.M. Shockley, E.F. Rauch, R.R. Chromik, S. Descartes, "TEM microanalysis of interfacial structures after dry sliding of cold sprayed Al-Al2O3," Wear 376, 1411-17 (2017) at DOI: 10.1016/j.wear.2016.12.052

reciprocating cycles which was confirmed to be of similar friction behavior and wear rate to the previous study.

TEM foils of the third body material in the wear tracks were prepared using an FEI FIB-SEM microscope using the *in situ* lift-out technique (see Figure 3). Samples were protected from gallium implantation using an electro-deposited carbon layer. The dimensions of the prepared TEM foils were approximately 10 µm x 10 µm. TEM was carried out in a Tecnai G2F20 S/TEM, working at 200kV, with a point-to-point resolution of 0.24nm. Energy-dispersive X-ray spectroscopy (EDS) was carried out on the TEM foils in a Hitachi SU-8000 SEM at 2.5 kV. Automated crystal orientation mapping (ACOM) was carried out in a TEM [12].

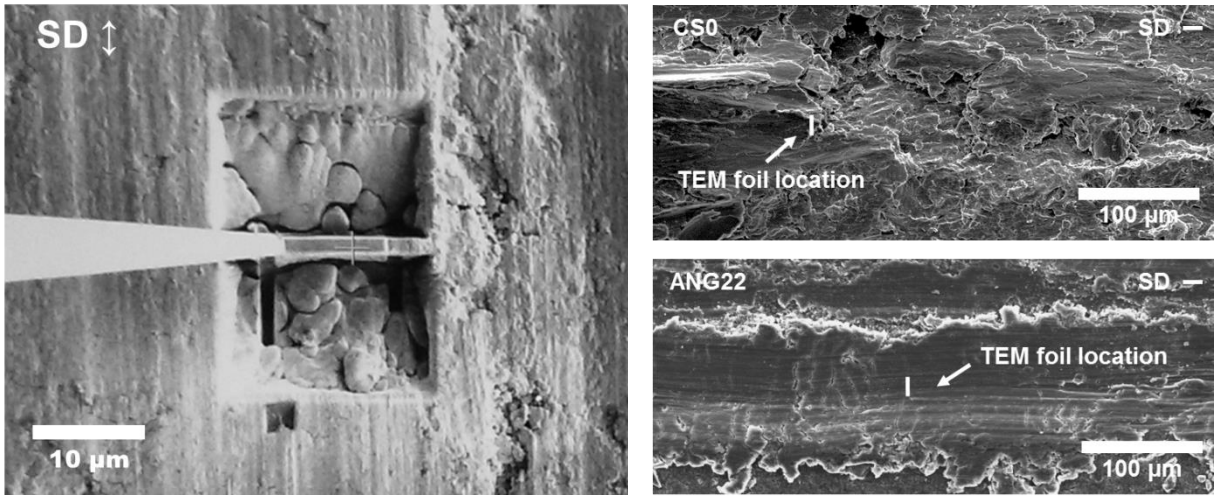

Figure 3: Left: liftout technique of TEM foil; right: wear track surfaces showing TEM foil liftout locations

3 Results and discussion

3.1 Friction, wear rates, and surface analysis

During the sliding wear tests, the friction coefficient fluctuated between 0.55 and 1.15 for sample CS0, initially starting high and then generally decreasing over the initial 300 cycles. The friction coefficient for ANG22 remained comparatively stable between 0.55 and 0.65. Wear rates of $0.02815 \pm 0.00263 \times 10^{-5}$ mm^3 N^{-1} m^{-1} were measured for CS0 and $0.00357 \pm 9.72843 \times 10^{-5}$ mm^3 N^{-1} m^{-1} for ANG22. Surface analysis of the wear track of sample CS0 revealed a series of uneven, smeared layers (see Figure 3, top right). In comparison, the wear track surface of sample ANG22 was covered in relatively smooth layers, with occasional cracking perpendicular to the sliding direction (see Figure 3, bottom right). The friction plots and wear rates compare favorably with numerous previous studies by the authors, which have studied in detail the correlations between friction events and the behavior of the third body at the sliding interface for these and similar samples [9, 10, 11]. The contrasting wear track surface morphology between CS0 and ANG22 are in similar agreement with previous studies.

This is a post-peer-review, pre-copyedit version of an article published in Wear. J.M. Shockley, E.F. Rauch, R.R. Chromik, S. Descartes, "TEM microanalysis of interfacial structures after dry sliding of cold sprayed Al-Al2O3," Wear 376, 1411-17 (2017) at DOI: 10.1016/j.wear.2016.12.052

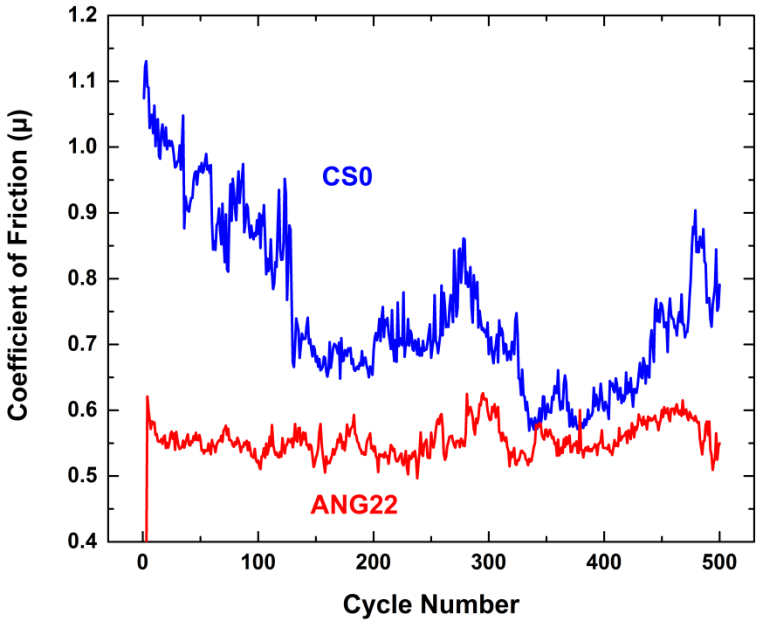

Figure 4: Friction coefficient of samples CS0 and ANG22

3.2 Microstructure of CS0

Low magnification TEM of sample CS0 revealed a layered microstructure consisting of clusters of multiple grain sizes (see Figure 5). The bottom region of the image shows larger grain sizes with a grain size gradient, separated from the rest of the microstructure by a series of horizontal cracks. Above these cracks the grain sizes were mixed, with regions of ultrafine and nanocrystalline grain sizes. The lower region is the deformed first body, where the grain size gradient has been documented previously [10]. The upper region is the third body, which was smeared over the first body during the adhesive wear process [10].

This is a post-peer-review, pre-copyedit version of an article published in Wear. J.M. Shockley, E.F. Rauch, R.R. Chromik, S. Descartes, "TEM microanalysis of interfacial structures after dry sliding of cold sprayed Al-Al2O3," Wear 376, 1411-17 (2017) at DOI: 10.1016/j.wear.2016.12.052

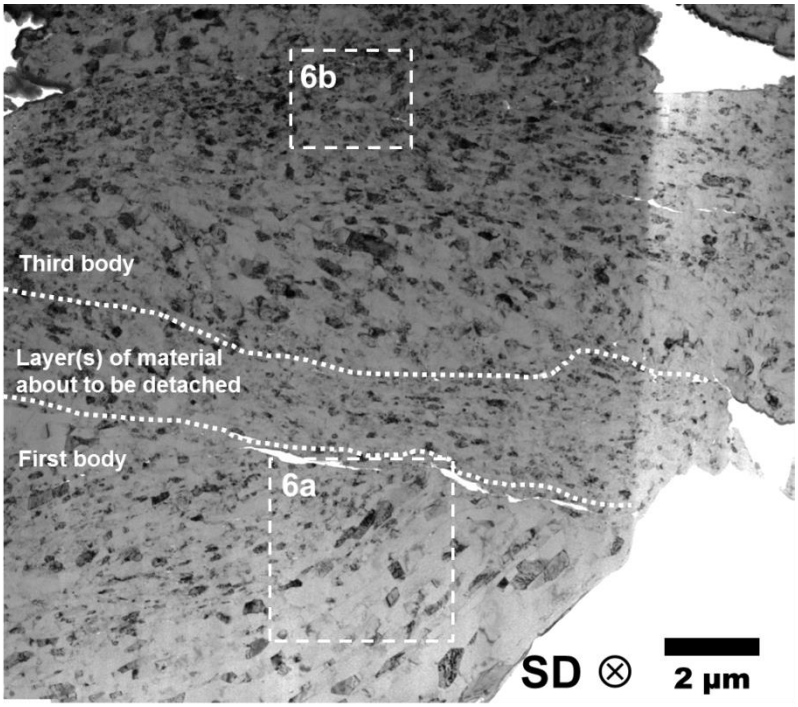

Figure 5: Low magnification TEM of sample CS0, with sliding direction perpendicular to the image. The lower region is the deformed first body layer, while the third body layer sits above it. Higher magnification images of the bound regions are shown in Figure 6.

The microstructure of the first body region of CS0 showed a grain size gradient indicative of plastic deformation (see Figure 6a). The smallest apparent grain sizes in the first body were on the order of roughly 50 nanometers. In the CS0 third body region, there are many grain sizes visible with the smallest on the order of about 20 nanometers (see Figure 6b). Electron diffraction reveals that no amorphous material is present, and that the material is entirely nanocrystalline aluminum.

This is a post-peer-review, pre-copyedit version of an article published in Wear. J.M. Shockley, E.F. Rauch, R.R. Chromik, S. Descartes, "TEM microanalysis of interfacial structures after dry sliding of cold sprayed Al-Al2O3," Wear 376, 1411-17 (2017) at DOI: 10.1016/j.wear.2016.12.052

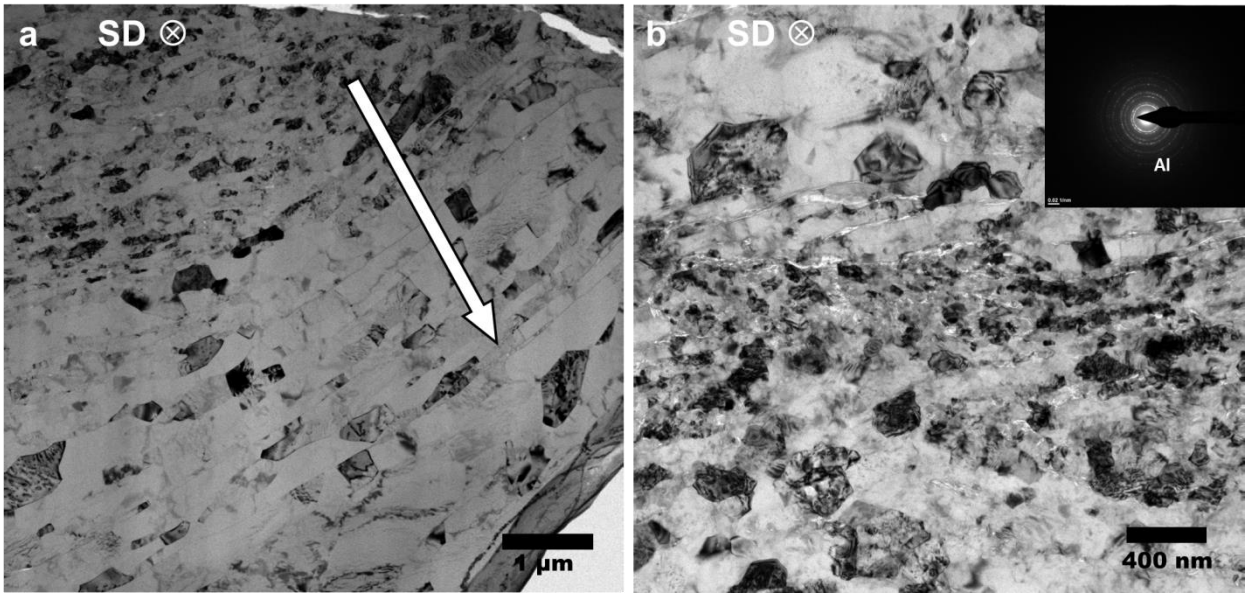

Figure 6: a) CS0 first body showing grain size gradient (white arrow); b) CS0 nanocrystalline region of third body with SAED (inset).

ACOM of the CS0 foil allowed for quantification of the differences in grain sizes between the first and third bodies (see Figure 7 and Figure 8). A high magnification ACOM of the third body region (Figure 7b) revealed a mix of nano-sized grains (<50 nm) and larger grains, with a mean grain size of 136 nm. A similar mapping of a first body region revealed a mean grain size of 324 nm. The average and maximum grain sizes increased with depth in the first bodies, forming a gradient of grain sizes, while the grain sizes within the third body varied considerably.

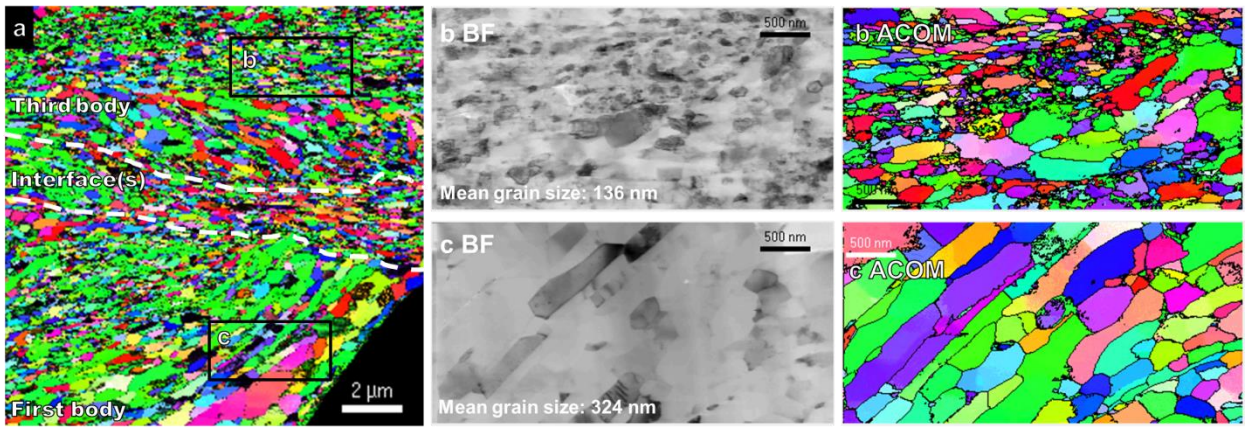

Figure 7: CS0 microstructure in (a) overall perspective of orientation mapping, (b) bright field and ACOM of a third body region, and (c) bright field (BF) and ACOM of a first body region. Grain sizes are calculated by area.

This is a post-peer-review, pre-copyedit version of an article published in Wear. J.M. Shockley, E.F. Rauch, R.R. Chromik, S. Descartes, "TEM microanalysis of interfacial structures after dry sliding of cold sprayed Al-Al2O3," Wear 376, 1411-17 (2017) at DOI: 10.1016/j.wear.2016.12.052

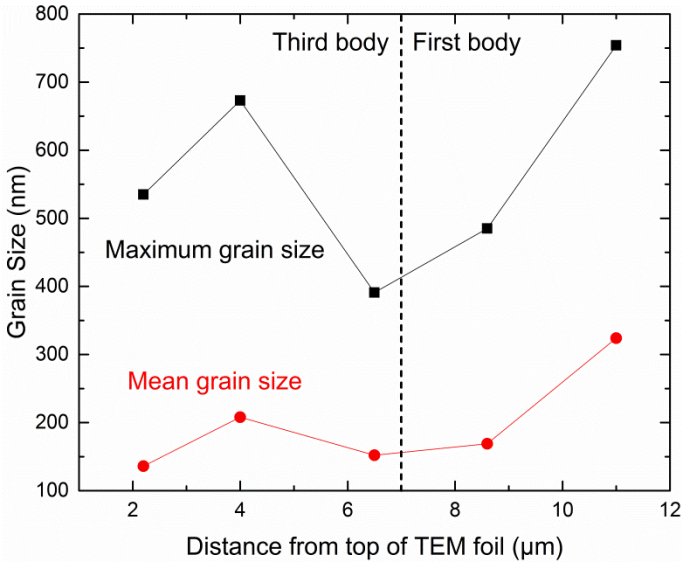

Figure 8: Maximum and mean (by area) grain sizes plotted versus distance from the top of the TEM foil. The grain size gradient in the first body is clearly highlighted.

EDS mapping highlighted the presence of elevated oxygen levels near the cracks in the first and third body microstructures (see Figure 9).

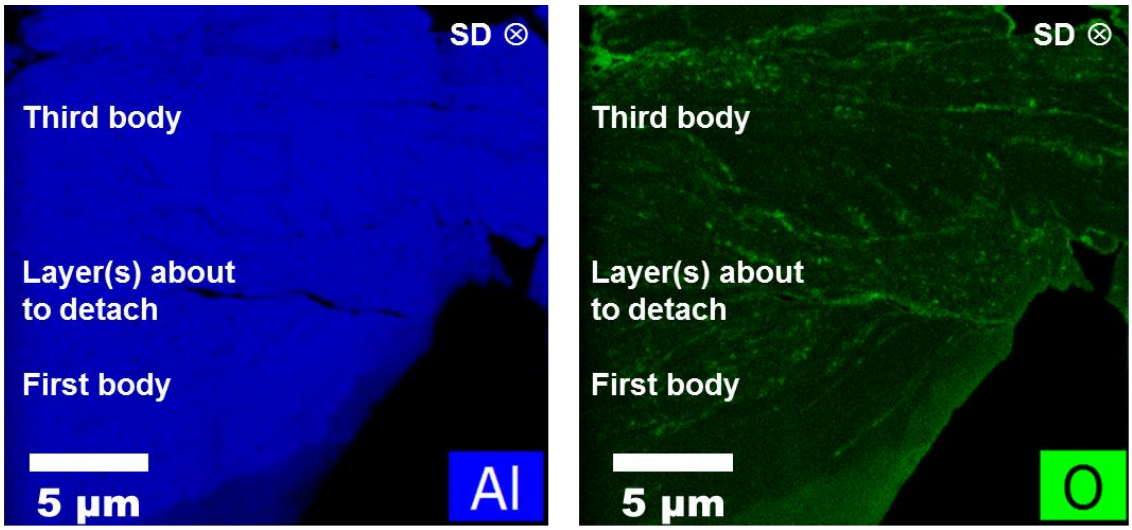

Figure 9: EDS mapping of aluminum Kα and oxygen Kα intensities for CS0. The region of low Al and high O signal in the bottom of each image represents thin areas of the foil.

3.3 Microstructures of ANG22

This is a post-peer-review, pre-copyedit version of an article published in Wear. J.M. Shockley, E.F. Rauch, R.R. Chromik, S. Descartes, "TEM microanalysis of interfacial structures after dry sliding of cold sprayed Al-Al2O3," Wear 376, 1411-17 (2017) at DOI: 10.1016/j.wear.2016.12.052

Low magnification TEM of sample ANG22 revealed distinct contrasts between the first and third body material (see Figure 10). In the first body, grain sizes remain more or less microscale until close vicinity of the third body material, becoming refined to no less than roughly 500 nm until immediately adjacent to the third body material. Third body material is present in discrete pieces embedded in the third body sitting at the sliding surface. Several pieces of third body material in Figure 10 detached and were lost during the FIB thinning process. No Al2O3 particles happened to be captured in the region where the FIB foil was extracted.

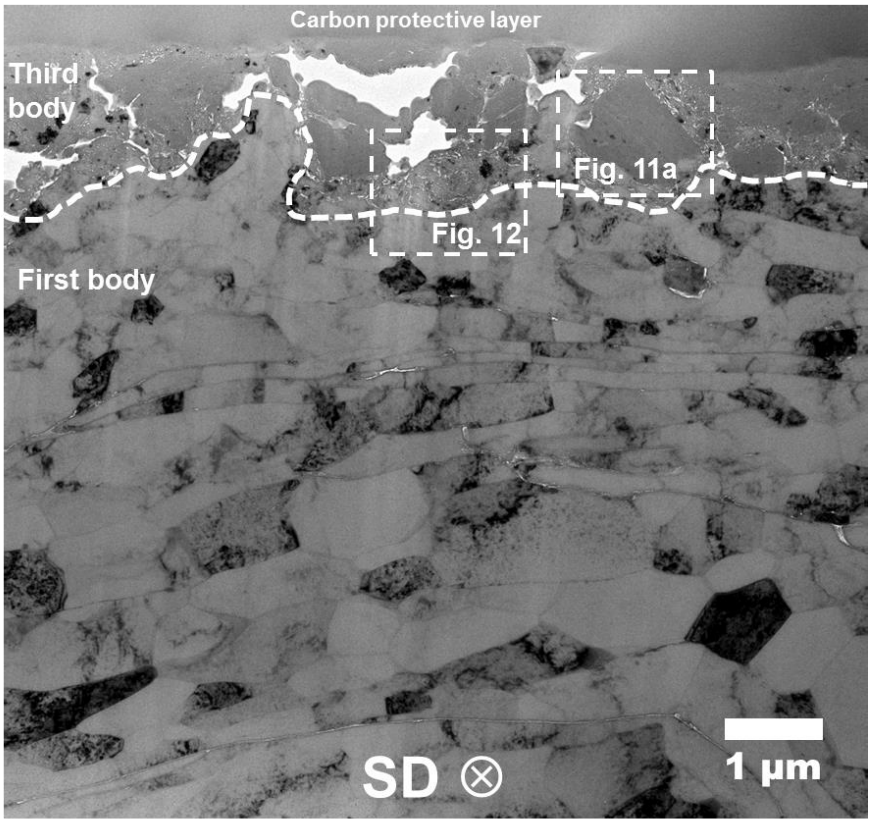

Figure 10: Low magnification TEM of sample ANG22, with sliding direction perpendicular to the image. The inset boxes are shown in Figures 11 and 12.

A discrete section of third body was analyzed by higher magnification TEM (see Figure 11). The severely deformed region between the first and third bodies was roughly 50 to 500 nm thick (Figure 11b), with a clear gradient of grain size between the two. High magnification TEM (Figure 11c) revealed that the microstructure of the third body particle consisted predominantly of an amorphous matrix with small, nanocrystalline (~5-20 nm) phases present. Selected area electron diffraction (pictured) and plane spacing measurements (not pictured) revealed that these phases within the amorphous matrix were aluminum.

This is a post-peer-review, pre-copyedit version of an article published in Wear. J.M. Shockley, E.F. Rauch, R.R. Chromik, S. Descartes, "TEM microanalysis of interfacial structures after dry sliding of cold sprayed Al-Al2O3," Wear 376, 1411-17 (2017) at DOI: 10.1016/j.wear.2016.12.052

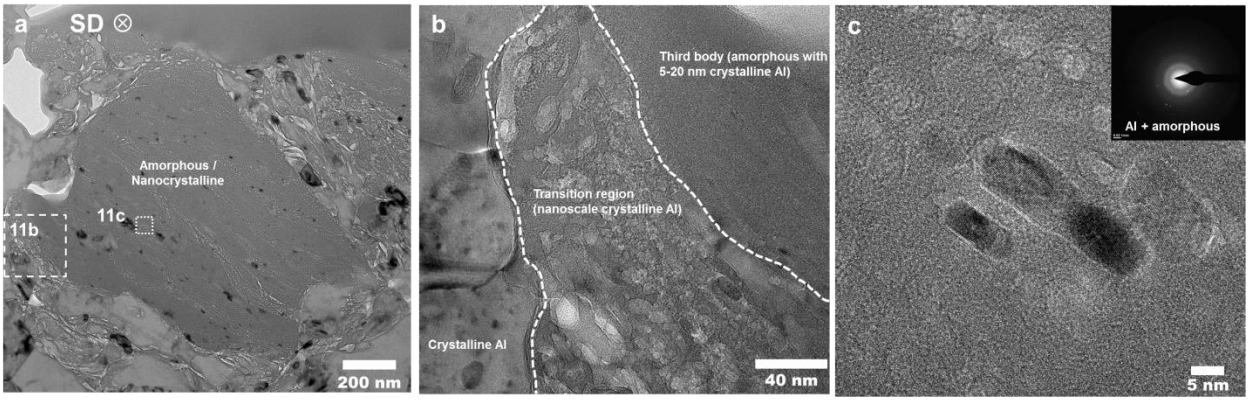

Figure 11: a) A piece of third body material in ANG22 with inset regions shown in 11b and 11c; b) a severely deformed region between first and third body showing a grain size gradient; c) high resolution TEM of a region within (a) with SAED (inset).

ACOM measurements of a similar transition region revealed a bimodal distribution of grain sizes between ultrafine (on the order of 200 nm) and nanocrystalline (5-30 nm) (see Figure 12).

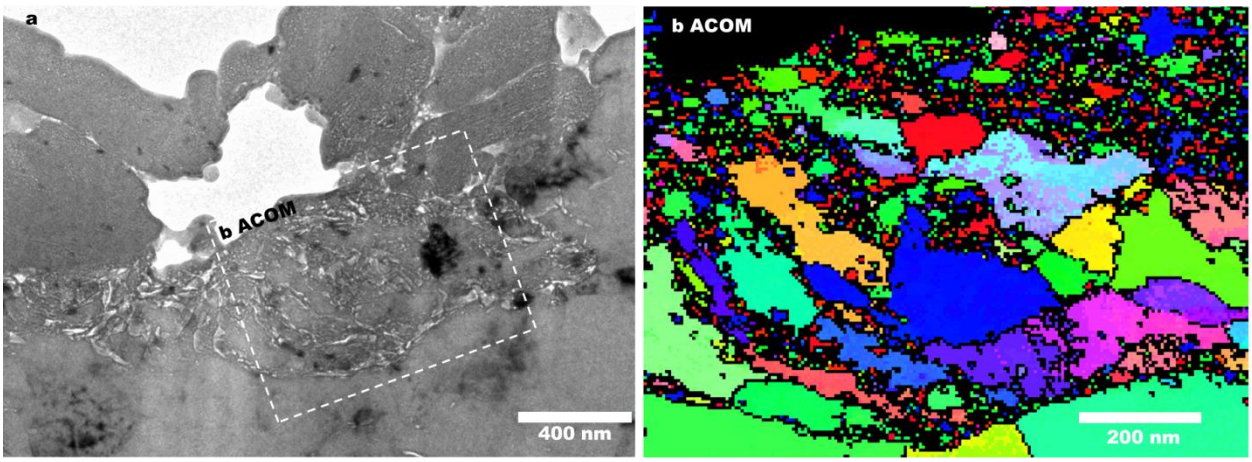

Figure 12: (a) A transition region adjacent to a missing third body region of ANG22 (lost during the ion milling process) and (b) ACOM of a selected region.

Various grains within the ANG22 first body showed signs of deformation, and misorientation mapping showed a continuous change of orientation throughout one such grain, which led into a low angle grain boundary (<5° misorientation) (see Figure 13).

This is a post-peer-review, pre-copyedit version of an article published in Wear. J.M. Shockley, E.F. Rauch, R.R. Chromik, S. Descartes, "TEM microanalysis of interfacial structures after dry sliding of cold sprayed Al-Al2O3," Wear 376, 1411-17 (2017) at DOI: 10.1016/j.wear.2016.12.052

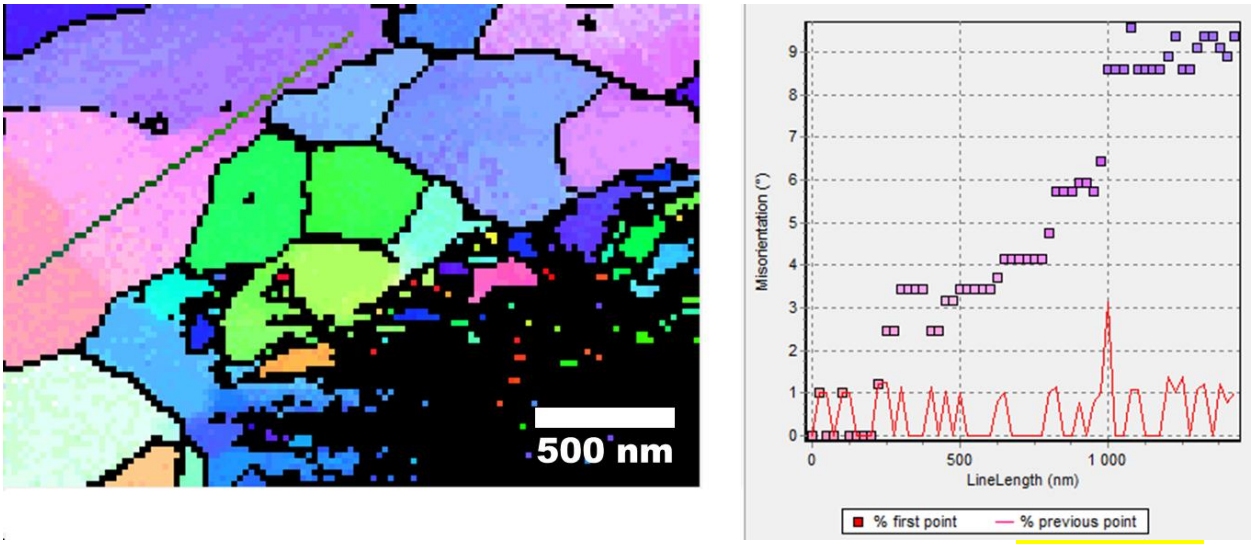

Figure 13: Misorientation mapping of a deformed aluminum grain within the aluminum first body of sample ANG22.

EDS mapping revealed high levels of oxygen in the third body layer, suggesting the amorphous layer is an amorphous oxidized aluminum (see Figure 14). Elevated oxygen levels were also observed in the interfacial regions near the third body particles, though they were lower than that of the third body themselves. No crystalline aluminum oxide was identifiable within the ANG22 third or first body microstructures according to SAED.

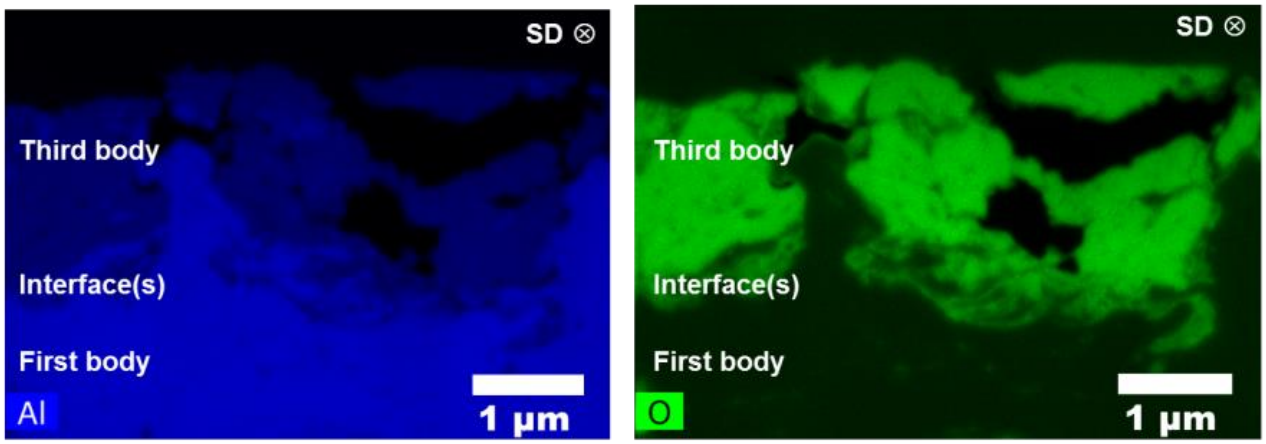

Figure 14: EDS mapping of aluminum Kα and oxygen Kα intensities in the ANG22 third body, the surrounding first body, and interfaces.

4.0 The influence of hard particles on the subsurface microstructural evolution

The transformations occurring at the sliding interface and the influence of the presence of Al2O3 particles thereof were described through TEM, EDS and ACOM analysis. The differing friction behaviour between CS0 and ANG22 was attributed to the formation of a smooth and coherent third body film for sample ANG22, which did not form for sample CS0. TEM microanalysis revealed that the third body material of CS0 consisted of a mixture, 10-30 µm thick, of a large

This is a post-peer-review, pre-copyedit version of an article published in Wear. J.M. Shockley, E.F. Rauch, R.R. Chromik, S. Descartes, "TEM microanalysis of interfacial structures after dry sliding of cold sprayed Al-Al2O3," Wear 376, 1411-17 (2017) at DOI: 10.1016/j.wear.2016.12.052

range of grain sizes (25-500 nm) and contained elevated oxygen residing at the many cracks and interfaces. That of ANG22 (3-5 µm thick) had a bimodal distribution of small Al grains (200 nm) and extremely small Al grains (~5-20 nm) embedded in a heavily oxidized, amorphous matrix. No α-Al2O3 was detected in the ANG22 third body, meaning its microstructure was formed entirely through deformation- and oxidation-driven microstructural changes. The presence of the initial Al2O3 led to the formation of an efficient, thin third body, not through incorporation of fragmented Al2O3 into the tribolayer, but rather by driving transformations within the aluminum itself.

Nanoindentation has previously revealed that CS0 the third body material is somewhat harder than the underlying first body (1.5 vs. 0.9 GPa), but the hardness of the ANG22 third body layer (3.8 GPa [10, 11]) is considerably higher. The elevated oxygen levels were found in both the CS0 and ANG22 third bodies, but for CS0, the oxygen was only found at cracks within the microstructure. This demonstrates the mechanical mixing occurring in the contact – detachment of material causes bare aluminum to be exposed, which rapidly oxidizes, and then third body material is smeared along the first body and other third body layers. Such detachment of layers of aluminum may be linked to shear instabilities in the subsurface [13], which then may become wear debris or become re-circulated and compacted into the contact during later cycles [10]. The high oxygen levels at the interfaces between layers of the CS0 third bodies also prevent complete metallic bonding across that interface, leading to easier detachment in subsequent cycles. Thus the CS0 third body is in a constantly evolving state of detachment and compaction. This contributes to the varying levels of strain and grain size observed the CS0 third body microstructure and to the unstable friction coefficient and high wear rate. Previous observations of elevated oxygen levels in the CS0 third body lacked the spatial resolution necessary to differentiate the fine cracks from the bulk of the third body, leading to speculation that mechanical milling of oxygen into the aluminum matrix was occurring [10], but this was apparently not the main mechanism. In contrast, the ANG22 third body contained consistently high oxygen levels throughout, suggesting that oxidation of the aluminum is taking place. The oxygen levels were lower than that observed in crystalline α-Al2O3 [10] and similarly, the ANG22 hardness, while elevated, was lower than that of crystalline α-Al2O3 (~20 GPa).

The formation of mechanically mixed third bodies during dry sliding of Al-MMCs is driven initially through subsurface strain and, secondarily, by chemical factors such as oxidation [6]. The stress under a spherical contact in these contact conditions is highest in the few microns immediately below the sample surface [14], and the variation of accumulated plastic strain in the subsurface can be related to the grain size gradient below the sliding surface [6, 15]. Among the various models for estimating subsurface strain, one of the simplest is a ratio:

$$\delta = \frac{D}{c(3^{1/2})} \quad (1)$$

where δ is the accumulated plastic strain, D is the initial grain size, and c is the refine grain size measured under in the subsurface [15]. The initial aluminum grain sizes of CS0 and ANG22 were similar (640 ± 370 nm [10]). The grain size gradient in the CS0 first body (Figure 5),

This is a post-peer-review, pre-copyedit version of an article published in Wear. J.M. Shockley, E.F. Rauch, R.R. Chromik, S. Descartes, "TEM microanalysis of interfacial structures after dry sliding of cold sprayed Al-Al2O3," Wear 376, 1411-17 (2017) at DOI: 10.1016/j.wear.2016.12.052

which has been previously shown to penetrate about 30 microns below the surface [10], indicates plastic straining to that distance. Using the mean grain sizes in Figure 8, this corresponds to strains as high as 2.7 in the third body and as low as 1.1 in the first body. The absence of such a broad gradient of grain size in ANG22 indicates that plastic straining was constrained to a much smaller distance due to the harder third body. Nonetheless, such a grain size gradient is visible in the transition region 50-500 nm thick between the first and third bodies of ANG22. The smaller grain sizes (as low as 5 nm) compared to CS0 implies a higher degree of strain, and the shorter distance over which they occur implies that a higher strain gradient was present in this region. Strain gradients are known to occur in the matrix of Al-MMCs in the vicinity of hard particles during straining [16], and the creation of geometrically necessary dislocations (GND) drives grain refinement at a faster rate in the vicinity of hard particles than elsewhere in the matrix [17, 18, 19, 20]. Mechanical mixing and detachment of this transition layer would account for the disordered, bimodal grain size distributions visible (Figure 12), and accounts for the higher oxygen levels at the edges of these regions (Figure 14). With time, this would result in the material being progressively oxidized from the outside, until finally small aluminum grains in the center of an amorphous matrix would be occasionally left over as islands (Figure 11c).

5 Conclusions

In the present study, TEM, EDS and ACOM analysis were used to reveal subsurface material transformations responsible for the differing tribological behavior of pure aluminum (CS0) and Al- 22 wt.% Al2O3 (ANG22) during dry sliding.

- Grain sizes in the CS0 were quantatively shown to be smaller in the third body compared to the first, and the grain size gradient in the first body was shown as well.
- Oxygen in the CS0 third body and near-surface first body was found primarily along crack surfaces between different layers, rather than incorporated into the crystal lattice.
- The ANG22 third body was confirmed to consist of amorphous, oxidized aluminum with small islands of crystalline aluminum.
- A grain size gradient was observed in the transition region between the ANG22 first and third bodies, as was high levels of oxygen along the edges of these regions, indicating that mechanical mixing and oxidation were responsible for the formation of the amorphous / nanocrystalline ANG22 third body.

Bibliography

[1] J. Davis, Ed., "Corrosion Behavior," in *Aluminum and Aluminum Alloys*, Materials Park, Ohio, ASM International, 1993, pp. 579-622.

[2] F. Gartner, T. Stoltenhoff, T. Schmidt and H. Kreye, "The cold spray process and its potential for industrial applications," *Journal of Thermal Spray Technology,* vol. 15, no. 2, pp. 223-232, 2006.

[3] E. Irissou, J.-G. Legoux, B. Arsenault and C. Moreau, "Investigation of Al-Al2O3 Cold

Spray Coating Formation and Properties," *Journal of Thermal Spray Technology,* vol. 16, no. 5-6, pp. 661-668, 2007.

[4] A. Alpas and J. Zhang, "Effect of SiC particulate reinforcement on the dry sliding wear of aluminium silicon alloys (A356)," *Wear,* vol. 155, pp. 83-104, 1992.

[5] A. Alpas and J. Zhang, "Effect of microstructure (particulate size and volume fraction) and counterface material on the sliding wear resistance of particulate-reinforced aluminum matrix composites," *Metallurgical and Materials Transactions A,* vol. 25A, pp. 969-983, 1994.

[6] R. Deuis, C. Subramanian and J. Yellup, "Dry Sliding Wear of Aluminium Composites - A Review," *Composites Science and Technology,* vol. 57, pp. 415-435, 1997.

[7] B. Venkataraman and G. Sundararajan, "The sliding wear behaviour of Al-SiC particulate composites - I. Macrobehaviour," *Acta Materialia,* vol. 44, no. 2, pp. 451-460, 1996.

[8] M. Ghazali, W. Rainforth and M. Omara, "A comparative study of mechanically mixed layers (MMLs) characteristics of commercial aluminium alloys sliding against alumina and steel sliders," *Journal of Materials Processing Technology,* vol. 201, pp. 662-668, 2008.

[9] J. Shockley, H. Strauss, R. Chromik, N. Brodusch, R. Gauvin, E. Irissou and J.-G. Legoux, "In situ tribometry of cold-sprayed Al-Al2O3 composite coatings," *Surface and Coatings Technology,* vol. 215, pp. 350-356, 2013.

[10] J. M. Shockley, S. Descartes, E. Irissou, J.-G. Legoux and R. R. Chromik, "Third Body Behavior During Dry Sliding of Cold-Sprayed Al-Al2O3 Composites: In Situ Tribometry and Microanalysis," *Tribology Letters,* vol. 54, pp. 191-206, 2014.

[11] J. M. Shockley, S. Descartes, P. Vo, E. Irissou and R. R. Chromik, "The influence of Al2O3 particle morphology on the coating formation and dry sliding wear behavior of cold-sprayed Al-Al2O3 composites," *Surface and Coatings Technology,* vol. 270, pp. 324-333, 2015.

[12] E. Rauche and L. Dupuy, "Rapid spot diffraction patterns identification through template matching," *Archives of Metallurgy and Materials,* vol. 50, no. 1, pp. 87-99, 2005.

[13] S. Kuo and D. Rigney, "Sliding behavior of aluminum," *Materials Science and Engineering A,* vol. 157, no. 2, pp. 131-143, 1992.

[14] G. Hamilton, "Explicit Equations for the Stresses beneath a Sliding Spherical Contact," *Journal of Mechanical Engineering Science,* vol. 197, no. 1, pp. 53-59, 1983.

[15] J. Dautzenberg and J. Zaat, "Quantitative determination of deformation by sliding wear," *Wear,* vol. 23, no. 1, pp. 9-19, 1973.

[16] P. Apps, J. Bowen and P. Prangnell, "The effect of coarse second-phase particles on the rate of grain refinement during severe deformation processing," *Acta Materialia,* vol. 51, no. 10, pp. 2811-2822, 2003.

[17] I. Gutierrez-Urrutia, . M. Muñoz-Morris and D. Morris, "The effect of coarse second-phase particles and fine precipitates on microstructure refinement and mechanical properties of severely deformed Al alloy," *Materials Science and Engineering: A,* vol. 394, no. 1-2, p. 399–410, 2005.

[18] I. Gutierrez-Urrutia, M. Muñoz-Morris and D. Morris, "Contribution of microstructural parameters to strengthening in an ultrafine-grained Al-7% Si alloy processed by severe

deformation," *Acta Materialia,* vol. 55, no. 4, pp. 1319-1330, 2007.

[19] M. Muñoz Morris, I. Gutierrez-Urrutia and D. Morris, "The effect of geometrically necessary dislocations on grain refinement during severe plastic deformation and subsequent annealing of Al–7% Si," *Materials Science and Engineering: A,* vol. 493, no. 1-2, p. 141–147, 2008.

[20] A. Mahato, N. Verma, V. Jayaram and S. Biswas, "Severe wear of a near eutectic aluminium–silicon alloy," *Acta Materialia,* vol. 59, no. 15, p. 6069–6082, 2011.

[21] E. Irissou and B. Arsenault, "Corrosion Study of Cold Sprayed Aluminum Coatings onto Al 7075 Alloy Substrates," in *Global Coating Solutions: Proceedings of the 2007 International Thermal Spray Conference*, 2007.